Insulator-metal transition of highly compressed carbon disulfide

Ranga P. Dias, Choong-Shik Yoo, Minseob Kim, and John S. Tse

Phys. Rev. B **84**, 144104 — Published 7 October 2011

DOI: 10.1103/PhysRevB.84.144104

Metallization of Highly Compressed Carbon Disulfide

Ranga P. Dias,[1] Choong-Shik Yoo*,[1] Minseob Kim,[1] and John S. Tse[2]

[1]Institute for Shock Physics, Department of Chemistry and Department of Physics, Washington State University, Pullman, Washington 99164, USA;

[2]Department of Physics and Engineering Physics, University of Saskatchewan, Saskatchewan, S7N 5E2, Canada.

*Corresponding author at csyoo@wsu.edu, (509) 335-2712

ABSTRACT

We present integrated spectral, structural, resistance, and theoretical evidences for simple molecular CS_2 transformations to an insulating black polymer with three-fold carbon atoms at 9 GPa, then to a semiconducting polymer above 30 GPa, and finally to a metallic solid above 50 GPa. The metallic phase is highly disordered 3D network structure with four-fold carbon atoms at the carbon-sulfur distance of ~1.70Å. Based on first principle calculations, we present two plausible structures for the metallic phase: α-chalcopyrite and tridymite, both of which exhibit metallic ground states and disordered diffraction features similar to that measured. We also present the phase/chemical transformation diagram for carbon disulfide, showing a large stability field of the metallic phase to 100 GPa and 800 K.

INTRODUCTION

Under high pressure, simple molecular solids transform into non-molecular (extended) solids as compression energies approach the energies of strong covalent bonds in constituent chemical species. As a result, it is common to observe the transformation of molecular solids into more compact extended structures with more itinerant electrons, which softens repulsive interatomic interactions at high density. Examples include insulator-to-metal transitions in O_2[1], Xe[2,3], and I_2[4] as well as molecular-to-nonmolecular transitions in CO_2[5] and N_2[6]. The latter transitions, on the other hand, open up the band gap, thereby, retarding the expected Mott insulator-to-metal transitions in these systems [7].

Carbon dioxide, for example, exhibits a richness of high-pressure polymorphs with a great diversity in intermolecular interaction, chemical bonding, and crystal structures. It ranges from molecular phases of I(Pa-3) [8] and III(Cmca)[9] to fully extended, polymeric phases of four-fold V [5,10], pseudo-six fold VI[11], coesite-like CO_2[12], and silica-like a-carbonia[13] above 40-60 GPa. These extended phases are polymorphs in structures similar to those of SiO_2, but with a substantially stronger covalent character in C-O bonds. At higher pressures of 100-200 GPa, all these extended phases of carbon dioxide transform into either amorphous solids at ambient temperature or ionic solids at high temperatures [14], not to a metallic phase. The absence of metallization, on one hand, reflects strong covalent nature of C-O bonds in these extended solids, which results in structural disorders to adapt the density increase at high pressures. The structural disorder, on the other hand, reflects an enhanced iconicity in C-O bonds – furthering the

separation of the band gap. Perhaps, the delicate balance between the structural disorder and the bond order is important for shifting the nature of the transition between ionization and metallization.

Carbon disulfide in comparison with its chemical analog CO_2, provides opportunities to exploit the relationship between the structural phase transition and the electronic metallization. Carbon disulfide crystallizes into molecular Cmca phase at < 1 GPa [15] – the isomorphic to CO_2-III. This Cmca phase is stable to 10 GPa and 540 K, above which it transforms to two-dimensional polymers such as a ladder polymer or a Bridgman black [16]. While carbon atoms in these polymers are mainly three-fold coordinated with sulfur atoms, a recent first-principles theory also predicts the stability of four-fold, quartz-like CS_2 phase above 20 GPa [17] - not been discovered.

Here, we report a series of structural and electronic phase transitions of molecular CS_2 to non-molecular phases with three- and four-fold carbon atoms and further to metallic phase above 50 GPa, using optical microscopy, Raman spectroscopy, electrical resistance, and x-ray diffraction measurements. The present results reveal structural and chemical analogies between CS_2 and CO_2 albeit significant differences in the chemical bonding and the stability field of these extended polymorphs at high pressures and temperatures.

METHODS

A Experimental Methods

The present study was based on a large number of experiments, more than twenty samples, all providing a consistent and reproducible set of Raman, electric resistance, and synchrotron x-ray scattering data. The sample was liquid CS_2 (99.99% from Sigma-Aldrich) loaded onto a membrane-driven diamond-anvil cell (m-DAC), using 1/3-carat, type Ia diamond anvils with a 0.3 (or 0.18 for higher pressures) mm culet. A 0.2 mm thick rhenium gasket was pre-indented to 30 μm and 130 (or 100) μm hole was electro-spark drilled at the center of the gasket. Raman spectra of CS_2 were obtained using a home-built confocal micro-Raman system based on a Nd:YLF laser (used the 2nd harmonic at 527 nm).

In electrical resistivity measurements, a fine alumina powder was mixed with epoxy and used to insulate the 5 μm thick platinum electrode from the metallic Re gasket. A 100 to 80 μm hole sample chamber was drilled at the center of the insulation powder (See Fig. 1). A four-probe method using 5 μm thick platinum electrodes was implemented with an average distance between opposite electrodes being around 40 to 50 μm. Direct current electrical resistance measurements were performed with 1 mA current, Lackshore 120 current source with switching polarity, and the voltage readout from Keithley 2000 DVM was recorded on a computer. For low resistance values AC technique was used at 13 Hz frequency with a 3 mA current from a Stanford Research SR830 digital lock-in amplifier.

Angle-resolved x-ray scattering data were collected at room temperature using micro-focused (~10x10 μm) monochromatic synchrotron x-ray at 16BMD/HPCAT

(λ=0.3682 Å) at the Advanced Photon Source. The x-ray scattering intensities were recorded on high-resolution 2D image plates over a large 2θ range between 0 and 40 degrees and then converted to 1D profiles using the Fit2D program. To investigate the structure in the amorphous phase, pair distribution function (PDF) analysis was performed on room temperature x-ray data by using the PDFGetX2. The background x-ray scattering was also measured from an empty cell after the experiments and was subtracted from the data to obtain the S(Q) of the sample (which will be shown later in Fig. 3). The S(Q) data was then Fourier transformed to obtain the g(r) (as shown in Fig. 3 inset).

B. Theoretical Methods

Crystal geometry optimization and electronic band structure calculations were performed with the First-Principles plane wave code VASP [18], employing the projected augmented wave potentials [19] with the Perdew-Burke-Ernzerhof functional [20]. The starting CS_2 chalcopyrite (*I-42d*) structure was adopted from the earlier study [21]. While the tridymite $P2_12_12_1$ structure for the extended phase-V of high pressure CO_2 [10] was used as the initial guess. Monkhorst-Pack *k*-point mesh of 16×16×16 and 6×8×8 were used in the electronic calculations for the chalcopyrite and tridymite structures, respectively. The convergence criterion for geometry optimization is the maximum force acting on an atom is less than 1.0×10^{-4} eV/Å.

To establish the stability of the chalcopyrite structure, phonon calculations using a *q*-point mesh of 4×4×4 were performed with the linear response code Quantum Espresso

[22]. Electron-phonon calculations using *q*-meshes of 3×3×3 and 4×4×4 show the coupling parameter is found to be very small. Owing to the large number of atoms in the primitive cell (8 C and 16 S) and the low space group symmetry, it was not feasible to perform linear response calculations for the phonon band structure and electron-phonon coupling parameter with our computational capability. Nevertheless, zone center phonons calculated with the linear response method using both VASP and Quantum Espresso and frozen phonon calculations using VASP on selected *q*-points reveal no imaginary frequency.

RESULTS

The most dramatic change in carbon disulfide under pressure is in its visual appearance (Fig. 1) from a transparent fluid to a molecular solid (*Cmca*) at 1 GPa (11) to a 1D black polymer of $(\text{-S-(C=S)-})_p$ with three-folded carbon atoms bonded to sulfur atoms (depicted as *CS3* phase) at 10 GPa [16], and to a reflecting polymer above 40-50 GPa.

Pressure-induced Raman and electric resistance changes (Fig. 2) indicate dramatic transformations of molecular carbon disulfide (*Cmca*) [7] to a previously known 1D black polymer of $(\text{-S-(C=S)-})_p$ with three-folded carbon atoms bonded to sulfur atoms at 10 GPa (depicted as *CS3* phase), and to a conducting polymer above 40-50 GPa. The Raman spectrum of molecular CS_2 consists of a symmetric stretching mode ν_s at 650 cm^{-1}, an overtone of S=C=S bending ν_b at 800 cm^{-1}, and a lattice mode at 100 cm^{-1}. Above 9 GPa, all of these modes disappear and, instead, two new broad peaks appear at ~430 cm^{-1}

and 500 cm^{-1} (see the inset), representing, respectively, the bending and stretching modes of (S-(C=S)-S) in a 1D polymeric configuration. Above 30 GPa, these two features merge into a single band at ~470 cm^{-1}, which can be attributed to the S-C-S bending mode in a 3D network structure made of CS_4 tetrahedra. The existence of this type of extended structure with four-fold carbon atoms was predicted for carbon disulfide above 20 GPa [17] and was found in its chemical analog, CO_2, above 40 GPa [5,10,21]. We, therefore, attribute the Raman change at 30 GPa to a structural phase transition to an extended carbon disulfide solid made of CS_4 tetrahedra (depicted as *CS4* phase).

The pressure-induced structural phase transitions accompany a large, seven-order, drop in electric resistance over a pressure range of 10 to 50 GPa, clearly suggesting an insulator-metal transition at ~50 GPa (Fig. 2). The conducting phase of carbon disulfide, especially in the *CS4* phase above 50 GPa, is opaque and highly reflective approaching the level of Pt metal (see Fig. 1). The measured resistance of the *CS4* phase at 50 GPa is less than 20 Ω which is typical for metals at this pressure in a DAC. The metallic nature of the *CS4* phase is consistent with its high optical reflectivity and its calculated electronic band structure later discussed.

The present x-ray diffraction data support the structural phase transitions of carbon disulfide to the 1D (*CS3*) and 3D (*CS4*) extended solids (Fig. 3). Below 10 GPa, the polycrystalline diffraction pattern of solid CS_2 is poor due to its large crystal grains with highly preferred orientations. Nevertheless, all the observed peaks can be indexed with the previously known *Cmca* structure of molecular CS_2 [15]. At higher pressures, those

sharp diffraction peaks weaken and broaden, becoming a few broad features centered at around 2.5, 3.3 and 4.3 $Å^{-1}$, indicating the transformation of CS_2 to a highly disordered solid. No diffraction feature is discernable for the presence of either sulfur or carbon, confirming that CS_2 does not decompose chemically. Note that all solid phases of sulfur (including *S-II* and *III* phases relevant to this pressure range) maintain high crystallinity well above 35 GPa (nearly to 200 GPa) at ambient temperatures [23].

The pair distribution function (PDF) profiles reveal the local structures of semiconducting *CS3* and metallic *CS4* phases (see the inset in Fig. 3). The first dominant peak can be assigned to the nearest carbon-sulfur distance (r1) [24]. For example, the peak at 1.32 (±0.05) Å at 9 GPa can be assigned to the C=S double bonds in molecular CS_2. The observed peak at around 1.70 (±0.05) Å at 27, 46 and 55 GPa can be assigned to the C-S single bonds in CS_4 tetrahedral with some partial C=S double bond characters [25]. The second dominant peak, on the other hand, can be assigned to the neighboring sulfur-sulfur distance (r2), which decreases from 4.08 and 3.25 Å at 9 GPa, corresponding to the two nearest S..S interatomic distances in the *Cmca* phase [26], to 2.99 and 3.15 Å at 27 GPa, corresponding to two different S..S distances in the *CS3* phase. It then collapses to 2.77 Å at 47-55 GPa. Interestingly, the ratio of r_1 and r_2, is ~1.63 at 55 GPa and is close to the ideal close-pack hexagonal structure c/a = 1.63, signifying its 3D network structure [27].

Based on the present (open circles) and previous (closed circles) data [11], we construct the phase/chemical transformation diagram of carbon disulfide in Fig. 4. It

highlights the metallization (in blue) and structural transitions (in black lines) for comparison and shows i) the structural transitions from molecular *Cmca* phase (CS_2) to a 1D black polymer (with three fold carbon atoms or *CS3* phase) at ~10 to 12 GPa and to a 3D extended polymer (*CS4* phase) at ~ 29 to 31 GPa, (ii) the insulator-to-metal transition occurring over a large pressure region between 29(31) GPa and 44(48) GPa at 300 K, and (iii) the decomposition of carbon disulfide to carbon and sulfur at high pressures and temperatures. The data at 710 K and 20 GPa signifies carbon disulfide decomposition to carbon and sulfur (*S-VI* phase [23]), which is confirmed by its characteristic Raman peak in the present resistive-heating experiments (Fig. 5a). Combining this and earlier data (at 530 K and ambient pressure), we establish the decomposition line of carbon disulfide with a positive slop (8.18 K/GPa - dashed line), indicating that the stability field of metallic *CS4* phase increases with increasing pressures. In fact, we confirmed that the *CS4* phase at 50 GPa was not decomposed to 725 K (Fig. 5b), the maximum temperature of the present resistive-heating experiments, but decomposes to carbon and *S-III* [23] upon laser-heating to higher temperatures (well above 1000 K) (Fig. 5c).

DISCUSSION

The present spectroscopic and diffraction results indicate the pressure-induced metallization of carbon disulfide at ~50 GPa, following a series of structural phase transitions from transparent molecular *CS2* phase to three-fold *CS3* phase at 10 GPa to four-fold *CS4* phase at ~30 GPa. The insulator-to-metal transition is *not* due to CS_2 decomposition or elemental sulfur, but occurs well in the stability field of highly disordered *CS4* phase as illustrated in Fig. 4.

To investigate further using first-principles density functional theory calculations, we determined the crystal and electronic structures of two plausible structures for highly disordered metallic *CS4* phase: those are, making the analogy with CO_2, the predicted chalcopyrite (*I-42d*) and observed tridymite ($P2_12_12_1$) structures of extended CO_2-V [10,21]. At ~50 GPa, the optimized tridymite and chalcopyrite structures have a similar density of 4.22 g/cm^{-3} well within the expected density range between extended CO_2 or diamond of ~3.56 g/cm^3 and sulfur-II of 4.26 g/cm^3 at 50 GPa [10,23]. The calculated diffraction profiles for both structures (tridymite at 55 GPa and chalcopyrite at 50 GPa in Fig. 3b) reproduced the observed major bands at Q =2.7 Å^{-1} and 4.5 to 5.5 Å^{-1}. However, the agreement is slightly better for the distorted tridymite structure because the asymmetry of the band profile from 4.5 to 5.5 Å^{-1} is correctly modeled.

The chalcopyrite structure is composed solely of the CS_4 tetrahedra with one unique C-S bond of 1.74 Å. The S-C-S valence angles from 103^o – 107^o are close to the ideal tetrahedron (Fig. 3b top). The tridymite structure, on the other hand, is highly distorted and consists of corner-sharing four (C1)- and three (C2)-fold coordinated carbon atoms at 52 GPa (Fig. 3b bottom). At 52 GPa, the C-S bond lengths vary between 1.68 and 1.86 Å with S-C-S angles from 100^o to 120^o. It is also significant that the CS_4 tetrahedra contain a relatively long C1-S bond of 1.86 Å as compared to the remaining 1.71, 1.75 and 1.78 Å. The trigonal arrangement around C2 is almost planar with two C2-S bonds of 1.71 Å and slightly shorter bond of 1.68 Å. The nearest C2…S contact distance is 2.10 Å at 52 GPa, which rapidly decreases with increasing pressure and collapses to 1.90 Å at 78 GPa.

Thus, above 78 GPa the tridymite structure is expected to become a fully four-coordinated structure made of highly distorted CS_4 tetrahedra with one long (1.9 Å) and three short (~1.7 Å) C-S bonds. Similarly, mixed three- and four-fold CO_2 layer structures have been proposed to be energetically competitive with fully four-fold structures at high pressures [28,29].

Over the pressure range from 20 – 60 GPa, the calculated enthalpy of tridymite is 0.3 to 0.4 eV/CS_2 higher than that of the chalcopyrite structure, but the energy difference decreases with increasing pressure (Fig. 6a). The both structures have a metallic ground state (Figs. 6b and 6c) as observed in experiments and are found to be dynamically stable. We found that the calculate electron-phonon parameter of the chalcopyrite structure is very small (Fig. 6d). The low symmetry and large number of atoms in the tridymite unit cell preclude calculations on the electron-phonon coupling parameter. However, the electronic band structure of the tridymite at 47 GPa, on the other hand, reveals two interesting features (Fig. 6): (i) the simultaneous presence of flat and dispersive bands near the Fermi level and (ii) a set of parallel bands along $\Gamma \rightarrow Y$ that may lead to possible nesting of the Fermi surface. These features have been suggested to favor superconductivity [30].

The present phase/chemical transformation diagram reveals the chemical analogy between carbon disulfide and carbon dioxide, sharing a similar polymorph in *Cmca* for molecular CS_2-I (or *CS2*) and CO_2-III phases and its transformation to non-molecular solids likely in tridymite-like structures. However, there exist some significant

differences between the two. For example, molecular CS_2 transforms into highly disordered three- and four-fold polymers above 10 GPa, which eventually metallizes above 50 GPa. The disordered structure of CS_2 with mixed three- and four-fold structures stays over a large pressure range (40 – 70 GPa), underscoring a substantial degree of ionic character in C-S bonds. On the other hand, CO_2-III transforms to various extended solids with primarily four-fold coordinated carbon atoms above 40 GPa and high temperatures; then, those extended solids transform into non-metallic amorphous solids above 80-200 GPa or extended ionic solids at high temperatures [14,31]. The structures of amorphous extended CO_2 solids have been suggested to have carbon atoms with mixed three- and four-fold coordination [14,29,31]. Therefore, the nature of structural disorder seems to be similar between the two, but their electronic structures are quite different (metallic vs. insulator with Eg>3.5 eV).

Finally, it is remarkable to note that highly disordered *CS4* phase shows extremely high metallic conductivity, similar to those of elemental metals. This is in a stark contrast to the most "metallic" organic polymers that exhibit barely metallic conductivity [32]. The poor conductivity in organic polymers is due to the fact that their electronic structures are dominated by disorder with short mean free paths approaching the atomic separation (*i.e.,* Ioffe-Regel criterion) [33]. In this regard, the origin of high metallic conductivity in highly disordered *CS4* phase is quite puzzling, which certainly deserves further experimental and theoretical studies on the exact nature of structural disorder and chemical bonding in this simple organic polymer of highly compressed carbon disulfide.

ACKNOWLEDGEMENTS

We thank Dr. Mathew Debessai for his technical assistance during the initial stage of the work. The x-ray work was performed using the HPCAT beamline at the APS, and we thank Dr. Y. Meng for her assistance. The present study has been supported by NSF-DMR (Grant No. 0854618) and DTRA (HDTRA1-09-1-0041).

REFERENCES:

1. G. Weck, P. Loubeyre and R. LeToullec, *Phys. Rev. Lett.* **88**, 035504 (2002).
2. R. Reichlin, K. E. Brister, A. K. McMahan, M. Ross, S. Martin, Y. K. Vohra, and A. L. Ruoff, *Phys. Rev. Lett*. **62**, 669 (1989).
3. K. A. Goettel, J. H. Eggert, I. F. Silvera, and W. C. Moss, *Phys. Rev. Lett.* **62**, 665 (1989).
4. K. Takemura, K. Sato, H. Fujihisa, and M. Onoda, *Nature* **423**, 971 (2003).
5. V. Iota, C. S. Yoo, and H. Cynn, *Science* **283**, 1510 (1999).
6. M. I. Eremets, A. G. Gavriliuk, I. A. Trojan, D. A. Dzivenko, and R. Boehler, *Nature Materials* **3**, 558 (2004).
7. A.K. McMahan and R. LeSar, *Phys. Rev. Lett*. **54,** 1929 (1985).
8. W.H. Keespm and J.W.L. Kohler, *Physica* **1**, 167 (1934).
9. K. Aoki, H. Yamawaki, M. Sakashita, Y. Gotoh, and K. Takemura, *Science* **263**, 235 (1994).
10. C. S. Yoo, H. Cynn, F. Gygi, G. Galli, V. Iota, M. F. Nicol, S. Carlson, D. Hausermann, and C. Mailhiot, *Phys. Rev. Lett.* **83**, 5527 (1999)
11. V. Iota, C.S. Yoo, J.-H. Klepeis, Z. Jenei, W. Evans, and H. Cynn, *Nature Mater*. **6**, 34 (2007); In phase VI, each carbon atom is surrounded by average six oxygen atoms in a highly distorted octahedral, but still maintains the sp^3 hybridization with four oxygen atom by disordering its position. This structural model of phase VI, however, has been challenged by the recent calculations in Refs. **28** and **29**, which suggest a layered carbonate structure with 3- and 4-fold coordinated carbon atoms
12. A. Sengupta and C.S. Yoo, *Phys. Rev. B* **82**, 012105 (2010).

13. M. Santoro, F.A. Gorelli, R. Bini, G. Ruocco, S. Scandolo, and W. A. Crichton, *Nature* **441**, 857 (2006).
14. C. S. Yoo, A. Sengupta, and M. Kim, submitted (2011).
15. N. C. Baenziger et al., *J. Chem. Phys*. **48**, 2974 (1968).
16. S. F. Agnew, R.E. Mischke and B.I. Swanson, *J. Phys. Chem*. **92,** 4201 (1988).
17. P. F. Yuan and Z. J. Ding, *J. Phys. Chem. Solids* **68**, 1841 (2007)
18. G. Kresse and J. Furthmüller *Comput. Mat. Sci.* **6**, 15, (1996).
19. G. Kresse, and J. Joubert, *Phys. Rev. B* **59**, 1758 (1999)
20. J. P. Perdew, K. Burke, and M. Ernzerhof, *Phys. Rev. Lett*. **77**, 3865, (1996).
21. S. Sera, C. Corazon, G.L. Chiarotti, S. Scandolo, and E. Tossatti, *Science* **284**, 788 (1999); this theoretical study suggests that carbonates involving special arrangements of CO_4 in layered amorphous and "m-chalcopyrite" structure are among the most stable structure for the extended phase of carbon dioxide.
22. P. Giannozzi, et.al., *J. Phys.: Condens. Matter*, **21**, 395502 (2009).
23. O. Degtyareva et al., *J. Chem. Phys.* **126**, 084503 (2007).
24. M. Powell, G. Dolling and B.H. Torrie, *Acta Cryst. B* **38**, 28 (1982).
25. G. Frapper and J-Y. Saillard, *J. Amer. Chem. Soc*. **122**, 5367 (2000).
26. M.M. Labes and L.F. Nichols, *Chem. Rev*. **79**, 1 (1979).
27. T. Ichikawa, *Phys. Stat. Sol. A*. **19,** 707 (1973).
28. S. Deng, A. Simon and J. Kohler, *Struct. Bond*, **114**, 103 (2005).
29. J. A. Montoya et al., *Phys. Rev. Lett.* **100,** 163002 (2008)
30. J. Sun et al., *Proc. Nat. Acad. Sci., USA* **106**, 6077 (2009).

31. C. S. Yoo, V. Iota, and H. Cynn, *Phys. Rev. Lett*. **86,** 444 (2001).

32. A. J. Heeger, *Angew. Chem. Int. Ed*. **40**, 2591 (2001).

33. A. F. Ioffe and A. R. Regel, *Prog. Semicond*. **4**, 237 (1960).

FIGURE CAPTIONS

Fig. 1 Microphotographs of carbon disulfide under high pressure showing its transformation from (a) transparent fluid to (b,c) molecular solid (*Cmca*) at ~1 GPa, to (d,e,g) black polymer above 10 GPa ((-S-(C=S)-)$_p$ or *CS3*), and eventually to (f,h) a highly reflecting extended solid above 48 GPa (*CS4*) at ambient temperature. The right-most image (h) illustrates the metallic reflectivity of CS_2 samples above 55 GPa similar to those of Pt probes in a four-probe configuration for resistance measurements.

Fig. 2 Pressure-induced Raman and electric resistance changes of carbon disulfide, showing the structural and electronic transitions. The inset shows subtle changes in Raman spectra in the 300-700 cm^{-1} region associated with the structural phase transitions at 10 and 30 GPa. The open and close symbols signify, respectively, the data taken during the pressure uploading and downloading.

Fig. 3 (Left) The background-removed structural factor S(Q) and radial distribution function G(r) (inset) of carbon disulfide obtained at several high pressures, showing the pressure-induced structural changes. (**Right**) The calculated structure factors of α-chalcopyrite (*I-42d*, top) and α-tridymite ($P2_12_12_1$, bottom), showing the two major features centered around 2.8 $Å^{-1}$ and 4.9 $Å^{-1}$ as observed in the experiments.

Fig. 4 The phase/chemical transformation diagram of carbon disulfide, showing the structural phase transitions, insulator-to-metal transition, and chemical decomposition,. Open circles signify data from the present study. The present high-temperature

experiments confirm the stability of *CS3* phase to 710 K at 22 GPa and at least 725 K at 50 GPa, which define the decomposition line of carbon disulfide to carbon and sulfur.

Fig. 5 The Raman spectra of ohmically heated carbon disulfide, showing thermal decomposition of CS_2 to carbon and sulfur (phase VI) at around 720 K at 22 GPa (a), but no apparent decomposition at 50 GPa to the maximum temperature of 723 K (b). The laser-heated carbon disulfide, on the other hand, decomposes to carbon and sulfur (phase III) at 30 GPa and > 1000 K (c).

Fig. 6 (a) The calculated enthalpies for the chalcopyrite (*I-42d*) and tridymite ($P2_12_12_1$) structure of CS_2 over a large pressure range from 20 to 60 GPa, showing that the chalcopyrite structure is more stable by about 0.3-0.4 eV/formula unit. (b) The electronic band structure of the chalcopyrite showing a metallic ground state. (c) The electronic band structure of the tridymite structure at 47 GPa showing the metallic nature and flat and parallel bands. (d) The phonon band structure and density of state for the chalcopyrite structure, showing the major Raman-active A1 phonon mode at 500 cm^{-1} and other IR modes at 700-800 cm^{-1}.

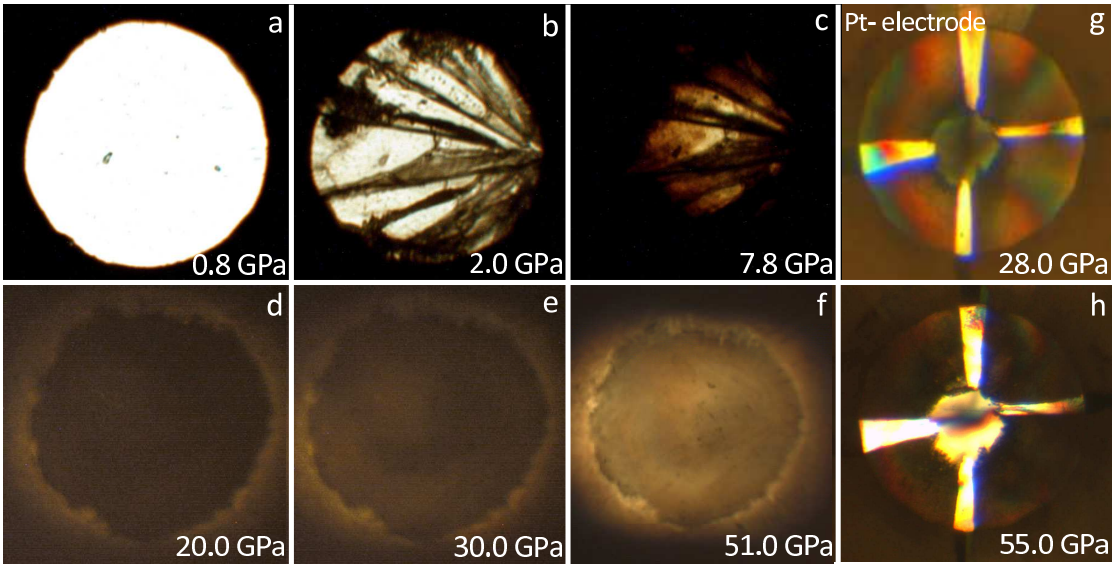

Fig. 1

Figure 1 LD13031B 13SEP2011

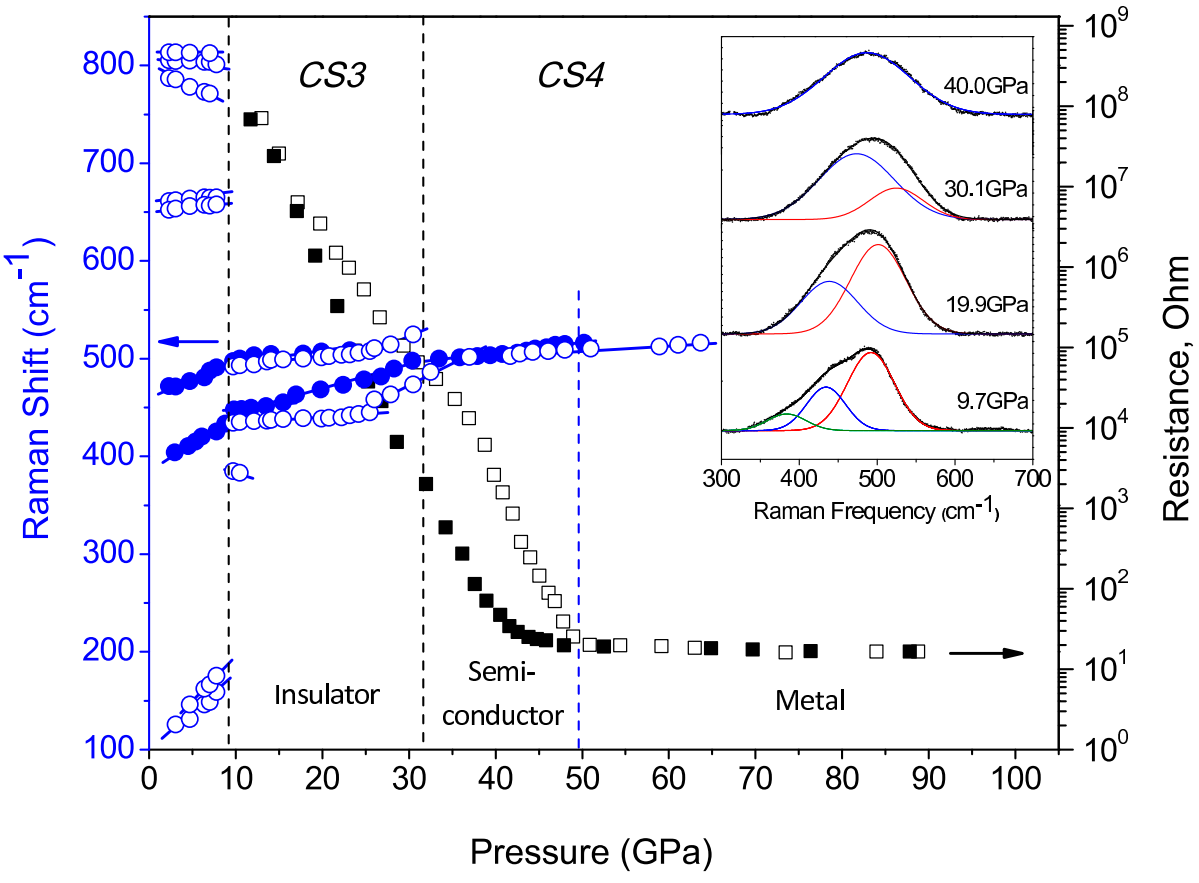

Fig. 2

Figure 2 LD13031B 13SEP2011

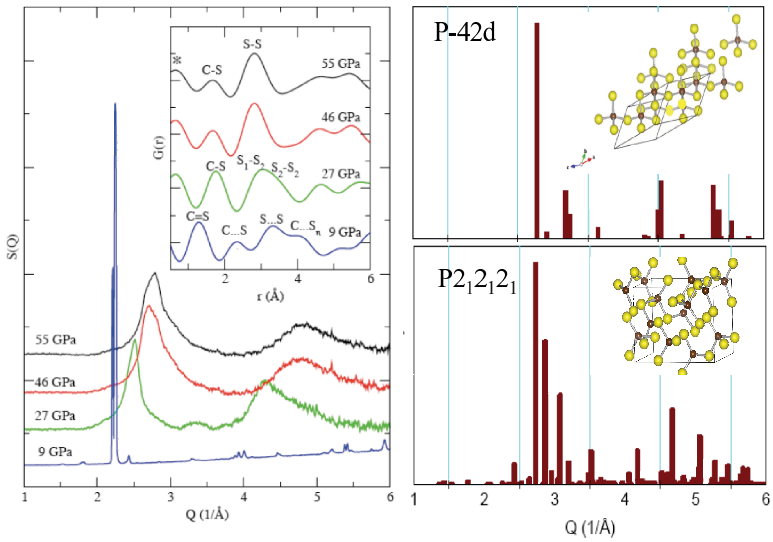

Fig. 3

Figure 3 LD13031B 13SEP2011

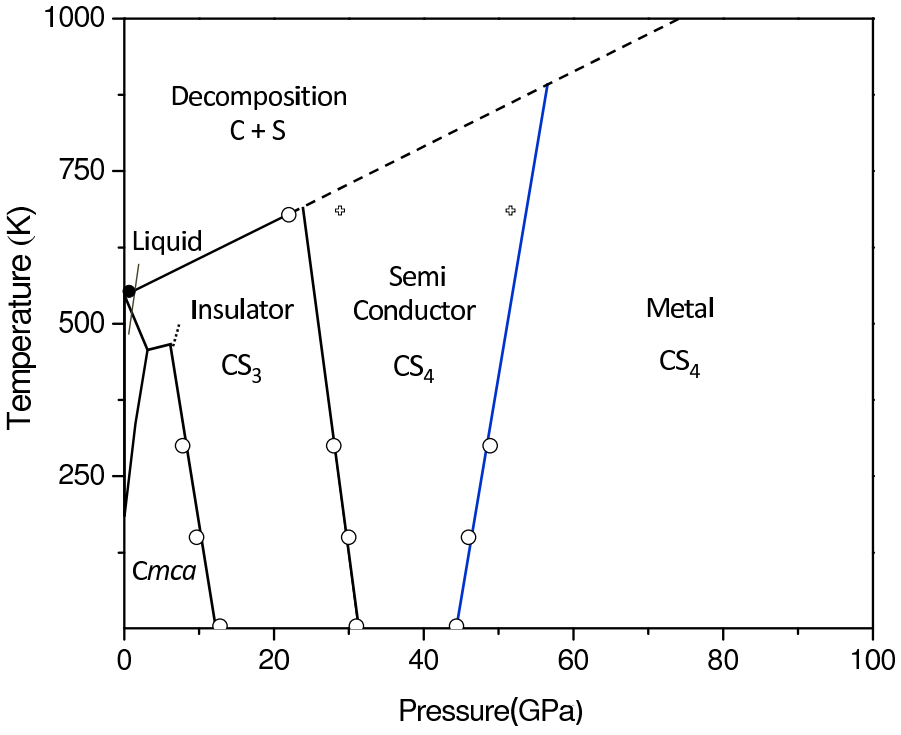

Fig. 4

Figure 4 LD13031B 13SEP2011

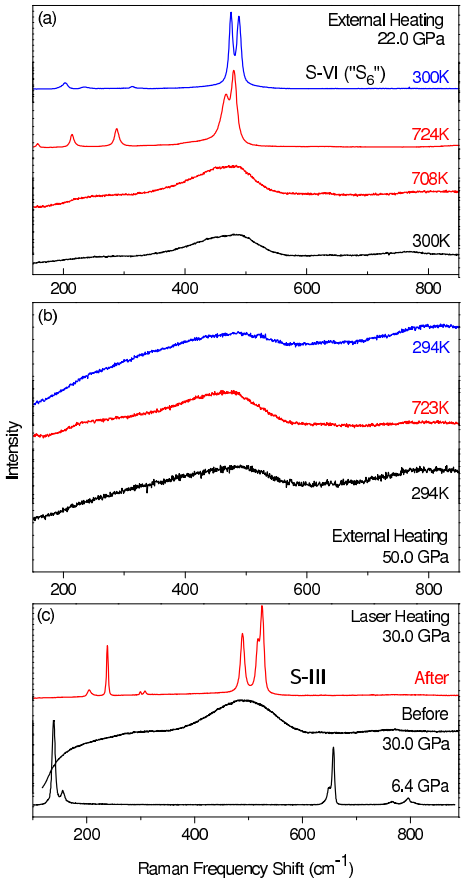

Fig. 5

Figure 5 LD13031B 13SEP2011

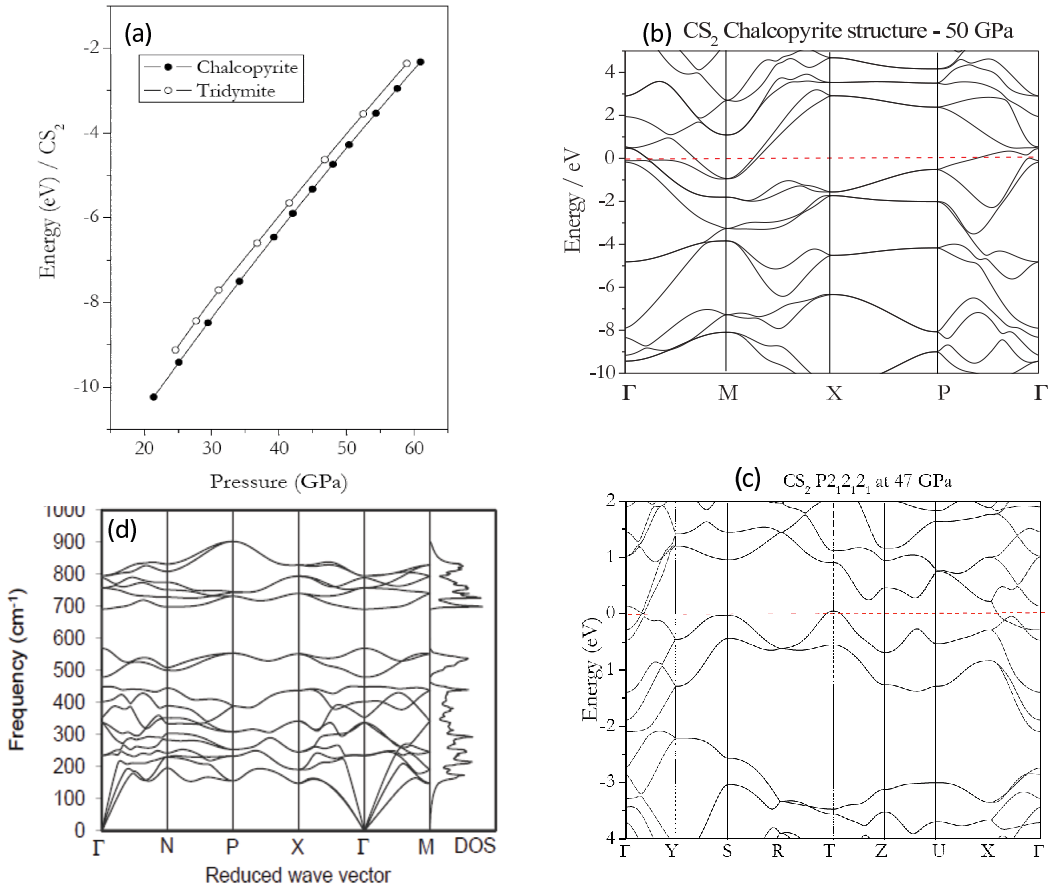

Fig. 6

Figure 6 LD13031B 13SEP2011